



Compressive Strength and Dimensional Accuracy of Portland Cement Mortar Made Using Powder-Based 3D Printing for Construction Applications

Ming Xia^(✉), Behzad Nematollahi, and Jay Sanjayan

Centre for Sustainable Infrastructure, Faculty of Science,
Engineering and Technology, Swinburne University of Technology,
Hawthorn, VIC, Australia
{mxia, bnematollahi, jsanjayan}@swin.edu.au

Abstract. An innovative methodology has recently been developed by the authors of this study for geopolymer formulations for the requirements and demands of commercially available powder-based 3D printers. In this study, the formulation is extended to conventional Portland cement to expand the scope of printable materials that can be used in the commercially available powder-based 3D printers for construction applications. A Portland cement-based powder composed of Portland cement, amorphous calcium aluminate and fine silica sand was developed for powder-based 3D printing process. Effects of different printing parameters including binder saturation level (100%, 135% and 170%) and shell to core ratio (1:1 and 1:2) on dimensional accuracy and compressive strength of the green specimens have been investigated. A compressive strength of up to 8.4 MPa was achieved for the ‘green’ 3D printed samples *before* any post-processing process. The results indicated that the increase in the binder saturation level and the change in the Shell/Core ratio from 1:1 to 1:2 significantly increased the compressive strength, but considerably reduced the linear dimensional accuracy of the green samples. The compressive strength and linear dimensional accuracy of the green samples exhibited an anisotropic behavior, depending on the testing direction.

Keywords: Powder-based 3D printing · Additive manufacturing
Portland cement · 3D concrete printing · Construction

1 Introduction

Three-dimensional (3D) printing, also known as additive manufacturing (AM) is a group of emerging techniques for fabricating a wide range of structures with complex geometries from digital models. The process involves of printing successive layers of materials that are formed on top of each other. Several industries including aerospace, automotive, biomedical have already explored the benefits of adopting this technology as an integral part of their product manufacturing process [1].

In the recent years, the construction industry has attempted to adapt this technology for construction applications owing to its potential use for direct construction of buildings and other complex structures of virtually any shape without the use of expensive formwork. Elimination of the formwork would result in considerable cost savings, as the formwork represents 35–60% of the cost of construction of concrete structures [2]. In addition, the elimination of formwork also reduces the amount of wastages in construction, and therefore improves sustainability in construction, since the formwork represents a significant source of waste as all of it is discarded sooner or later.

To date, the construction industry has explored two different 3D concrete printing (3DCP) techniques. One of these techniques is extrusion-based 3DCP, which is analogous to fused deposition modeling (FDM) method that extrudes cementitious material from an extruder mounted on a gantry, crane or a robotic arm to print a concrete component layer-by-layer. Recently the authors of this study developed a 3D printable fly ash-based geopolymers suitable for extrusion-based 3DCP for construction applications [3, 4].

Another technique is powder-based 3DCP, which is capable of making complex structures with subtle details and intricate shapes. Figure 1(a) schematically demonstrates the powder-based 3DCP technique. A thin layer of powder is spread over the powder bed surface. Subsequently, binder droplets are selectively applied on the powder layer by a print-head, causing powder particles to bind to each other. Repeating the described steps, the built part is completed and removed after a certain drying time and unbound powder is removed by using an air blower. One of the advantages of this technique is that over-hanging structures can be made without the necessity for using a supporting structure. This technique is an off-site process, which is highly suitable for manufacture of customized building components. Examples of technologies developed based on the powder-based 3DCP technique include D-shape [5] and Emerging Objects [6].

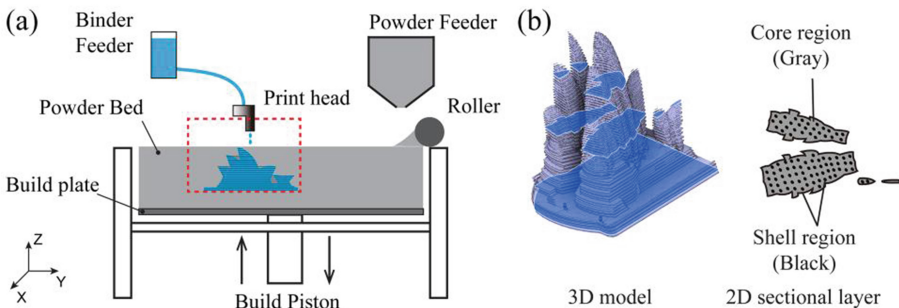


Fig. 1. (a) Schematic illustrations of powder-based 3DCP, (b) Schematic illustration of binder saturation.

Although the powder-based 3DCP technique can offer several advantages in the construction industry, there are a number of challenges to be overcome before the technique is fully utilized. One of the main challenges is that the proprietary printing materials that are typically used in the commercially available powder-based 3D

printers are not suitable for the construction applications. To tackle this limitation, the authors of this study have been working on developing innovative methodologies for formulating geopolymer based materials which can be used in the commercially available powder-based 3D printers for construction applications. Geopolymer is a sustainable alternative to conventional Portland cement. It is synthesized by alkaline activation of fly ash and/or slag, being industrial by-products of coal power stations and iron manufacture, respectively [7]. The authors of this study have recently developed several slag/fly ash-based geopolymer formulations suitable for powder-based 3DCP for construction applications [2, 8–11].

Conventional Portland cement has been considered as the master construction material for its high strength and stability as well as its low cost for over 100 years, and will probably be produced and used for at least the next 100 years [12]. However, the setting characteristics of Portland cement limit its use for powder-based 3DCP. Few studies have reported the use of other types of cementitious materials. For instance, Gibbons et al. [13] conducted a preliminary study to investigate the feasibility of using a mixture of poly vinyl alcohol and rapid hardening Portland cement (RHPC) for powder-based 3DCP process for manufacture of biomedical implants. The printed specimens exhibited a maximum modulus of rupture of 2.4 MPa after 26-day water immersion at ambient temperature. The low strength of the developed RHPC powder limits its use for construction applications. Maier et al. [14] investigated a mixture of flash-setting calcium aluminate cement (CAC) for powder-based 3D printing to fabricate a bone regeneration scaffold. A compressive strength of up to 20 MPa was reported for the printed specimen after 3-day water immersion. The relatively high cost of the developed CAC powder (as compared to conventional Portland cement) may limit its use for large-scale construction applications. To the best of the authors' knowledge no study has yet been reported the use of conventional Portland cement based materials for powder-based 3D printing for construction applications. This study aims to fill this knowledge gap by developing a new printable Portland cement-based material to expand the severely limited scope of cementitious materials that can be used in the commercially available powder-based 3D printers for construction applications.

In the powder-based 3DCP process, binder saturation is a decisive parameter that directly affects the binder/powder interaction [11], which is somewhat similar to water-to-cement ratio in the conventional concrete casting process. The binder saturation is defined as the ratio between the volume of deposited liquid binder (V_{Binder}) and the volume of pores in the powder bed (V_{Pores}). As schematically illustrated in Fig. 1(b), two sub-variables of the binder saturation are employed in the powder-based 3D printers, namely shell and core. These two sub-variables are used to be able to print a sample in a short time, providing adequate stability and avoiding oversaturation which can lead to distortion [15, 16]. The shell refers to the region comprising the edges of the sample and parts of the interior area within the edges of the sample. The core refers to the remaining interior areas within the edges of the sample. The high binder saturation results in bleeding of the binder into the surrounding powder. However, if the binder saturation is too low, the printed sample would have extremely weak green strength owing to the poor bonding between particles of the powder [17]. It is therefore necessary to understand the quantitative influence of the binder saturation on the properties of powder-based 3D printed samples. This study investigates the quantitative effects of

the binder saturation level and shell to core ratio on dimensional accuracy and compressive strength of 3D printed specimens using the novel Portland cement-based material.

2 Experimental Procedures

2.1 Materials

A conventional Portland cement conforming to the Australian Standard, AS 3972 general purpose (Type GP) cement was used in this study. The percentages of C_3S , C_2S , C_3A and C_4AF as the main constituents of Portland cement were 57.59%, 14.87%, 4.10% and 13.94%, respectively. A small amount of an accelerating additive was used to reduce the setting time of Portland cement, making it suitable for the powder-based 3DCP process. A high purity fine silica sand with an average particle size of 184 μm supplied by TGS Industrial Sand Ltd., Australia was also used in this study to function as an inert filler in the Portland cement-based powder to improve its printability. The raw materials were thoroughly dry mixed for 10 min in an Eirich mixer to achieve a homogenous mixture (visually assessed). The particle size distribution (PSD) of the developed Portland cement-based powder is given in Fig. 2. The PSD analysis result showed the average particle size, D_{10} , D_{50} and D_{90} values of the powder were 39.43 μm , 0.69 μm , 17.15 μm and 69.79 μm , respectively.

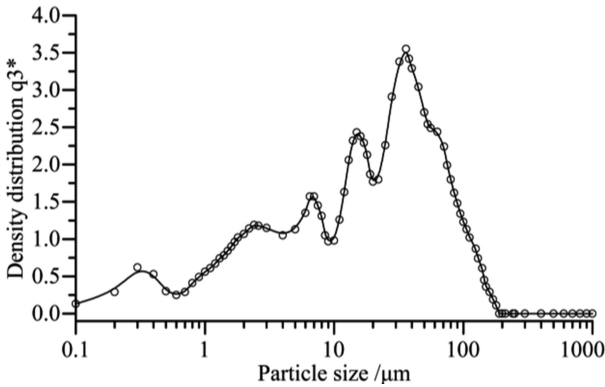


Fig. 2. Particle size distributions of the developed printable Portland cement-based powder.

2.2 Printing Process and Test Methods

3D Printing Process. A commercial powder-based 3D printer (Zprinter[®] 150) manufactured by Z-Corp, USA was used in this study. A commercial clear binder solution (Zb[®] 63) with a similar viscosity to pure water supplied by the printer's manufacture was used in this study. Details of the Zprinter[®] 150 and Zb[®] 63 binder can be found in the authors' previous work [8].

Figure 3 presents the 3D printed specimens using the developed Portland cement-based powder. A 20 mm cube specimen was printed to characterize dimensional accuracy and compressive strength of 'green' specimens. The green specimen refers to printed sample before any post-processing. An Opera House model with intricate shape was also designed and printed to demonstrate the feasibility of using the developed Portland cement-based powder for printing components with complex geometry. The powder layer thickness was set to 0.1016 mm. Three binder saturation levels of 100%, 135% and 170% and two shell to core ratios of 1:1 and 1:2 were selected in this study. The printed specimens were left within the powder bed for 2 h, and then de-powdering process was performed using a compressed air blower to remove the unbounded powder.

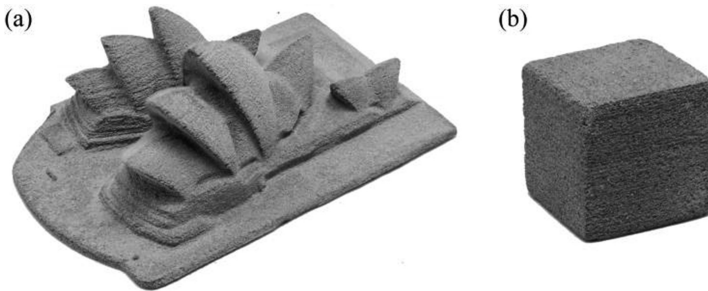


Fig. 3. 3D printed samples using the developed Portland cement-based powder (a) Opera House, (b) 20 mm Cubic structure.

Linear Dimensional Accuracy. A digital Vernier caliper with an accuracy of up to 0.01 mm was used to measure the dimensions of green cubic samples in three directions, namely X-direction (the direction of binder jetting), Y-direction (the direction of powder layer spreading) and Z-direction (the direction of layer stacking). The linear dimensional error was calculated based on the following equation:

$$Error = L_{actual} - L_{nominal} \quad (1)$$

Where L_{actual} is the measured length, whereas $L_{nominal}$ is the length of the digital model. A population of 10 samples for each testing direction was used. For each sample, three measurements were taken for each testing direction and the mean error values were calculated to assess the linear dimensional accuracy.

Compressive Strength. The compressive strengths of green cubic samples in both X-direction and Z-direction were measured under load control at the rate of 0.33 MPa/s. A population of 10 samples for each testing direction was used.

3 Results and Discussions

3.1 Linear Dimensional Accuracy

The primary benefit offered by the powder-based 3DCP process is the capability of producing building components with intricate shapes without the use of expensive formwork. One of the important factors that define the printability of a newly developed powder system is the printing accuracy. Figure 4 presents the results of the linear dimensional accuracy of green cubic samples.

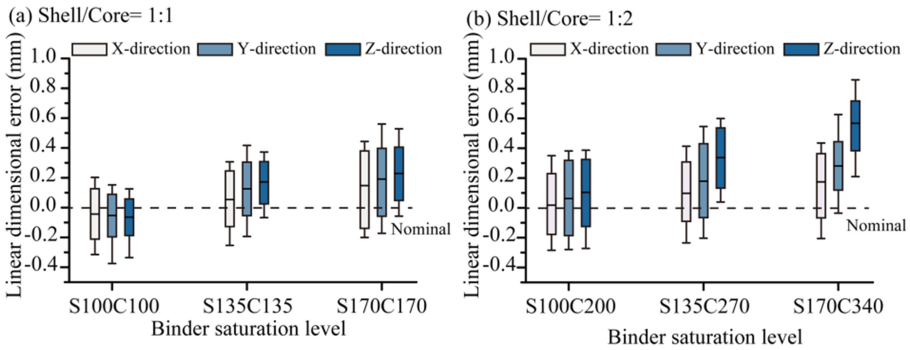


Fig. 4. Linear dimensional accuracy results of green cubic specimens printed with (a) Shell/Core = 1:1, (b) Shell/Core = 1:2. (Box: Mean \pm standard deviation; Whisker: Minimum to Maximum).

According to Fig. 4, the mean error values of the samples printed with saturation levels of 135% and 170% in all directions were always greater than zero. This indicates that the measured dimensions of printed samples in all directions were more than those of the digital model. This pattern is true regardless of the shell to core ratio. With regards to the samples printed with a saturation level of 100%, the measured dimensions of the samples printed with Shell/Core of 1:1 were less than the digital model, whereas the measured dimensions of the samples printed with Shell/Core of 1:2 were more than the digital model.

It should be noted that an anisotropic phenomenon was observed regarding the linear dimensional accuracy of the green samples depending on the testing directions. For all binder saturation levels, the Z-direction had the highest mean error values. In other words, regardless of the binder saturation level, the Z-direction had always the lowest linear dimensional accuracy. This phenomenon is more pronounced in the samples printed with Shell/Core of 1:2. This anisotropic phenomenon might be associated with the different rates of binder penetrating in vertical (Z) direction and spreading in lateral (X and Y) directions [15, 18]. On the other hand, for all binder saturation levels, the X-direction had the lowest mean error values, thereby the highest linear dimensional accuracy. This may be because the X-direction (i.e. the binder jetting direction) is not affected by the powder spreading that takes place in Y-direction.

As can be seen in Fig. 4, the increase in the binder saturation level considerably increased the mean error values in all directions. For example, for the green samples printed with Shell/Core of 1:1 the mean error value in Z-direction significantly increased from -0.07 ± 0.08 mm in the case of S100C100 to 0.24 ± 0.17 mm in the case of S170C170. In other words, the increase in the binder saturation level significantly reduced the linear dimensional accuracy of the green samples in all directions.

According to Fig. 4, the change in the Shell/Core ratio from 1:1 to 1:2 significantly increased the mean error values in all directions. This is true regardless of the binder saturation level. For instance, for the samples printed with Shell/Core of 1:1 the mean error value in Z-direction significantly increased from 0.13 ± 0.23 mm in the case of S170C170 to 0.57 ± 0.18 mm in the case of S170C340 with a Shell/Core of 1:2.

In summary, it can be concluded that the increase in the binder saturation level and/or the shell to core ratio significantly reduced the linear dimensional accuracy of the green samples printed using the developed Portland cement-based powder. This might be explained by the bleeding mechanism [19], since at higher binder saturation level the excess binder spreads outside the edges of the printed sample, which results in a reduction of the linear dimensional accuracy.

3.2 Compressive Strength

Figure 5 shows the compressive strength of green samples printed using the developed Portland cement-based powder in both X-direction and Z-direction.

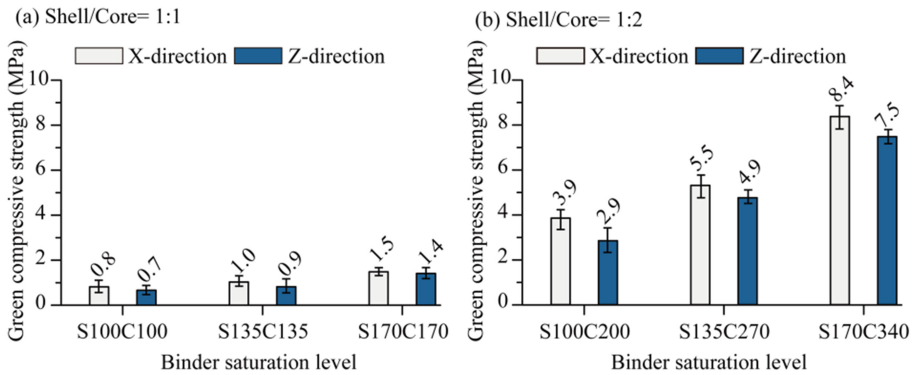


Fig. 5. Compressive strength of green cubic specimens printed with (a) Shell/Core = 1:1, (b) Shell/Core = 1:2.

As is shown in Fig. 5, an anisotropic phenomenon was observed regarding the compressive strength of the green samples depending on the loading directions. Regardless of the saturation level and shell to core ratio, the compressive strength was always higher in X-direction than in Z-direction. The anisotropy effect was more pronounced in the samples printed with Shell/Core of 1:2 as compared to Shell/Core of 1:1. For example, the compressive strength of the green samples printed with

S100C100 in X-direction was 14% higher than that in Z-direction. However, the compressive strength of the green samples printed with S100C200 in X-direction was 34% higher than that in Z-direction. This anisotropic phenomenon might be related to the preferential orientation of the powder particles during the powder spreading process [18].

According to Fig. 5, the change in the Shell/Core ratio from 1:1 to 1:2 significantly increased the compressive strength of the green samples. This is true regardless of the testing direction and binder saturation level. It is interesting to note that the rate of increase in the compressive strength of the green samples in X-direction was higher than in Z-direction. For instance, in X-direction the compressive strength of S100C100 samples was 4.9 times lower than that of the S100C200 samples. However, the corresponding value in Z-direction was 4.1 times. The green samples printed with Shell/Core of 1:1 exhibited relatively low compressive strength ranging from 0.7 to 1.5 MPa, depending on the testing direction and saturation level. However, it should be noted that the strength of all green samples printed with Shell/Core of 1:1 was already more than enough for the de-powdering process.

In both directions, the increase in the binder saturation level significantly increased the compressive strengths. However, the rate of increase in the compressive strength of the green samples with Shell/Core of 1:2 was higher than that with Shell/Core of 1:1. For instance, for Shell/Core of 1:1 and in X-direction the compressive strength of S170C170 samples was 1.9 times higher than that of S100C100 samples. However, the corresponding value for the Shell/Core of 1:2 is 2.15 times.

The inferior compressive strength of the green samples with lower binder saturation level and shell to core ratio is probably due to incomplete hydration process, which results in a weak bond between powder particles. Higher binder saturation level and core saturation use a higher volume of binder during the printing process, resulting in superior bonding between the powder particles.

4 Conclusions

A novel printable Portland cement-based powder was developed in this study which can be used in the commercially available powder-based 3D printers for the construction applications. The influence of binder saturation level and shell to core ratio on the linear dimensional accuracy and compressive strength of the green printed specimens was investigated. The following conclusions are drawn:

1. The increase in the binder saturation level and/or the core saturation significantly reduced the linear dimensional accuracy of the green samples. This is true regardless of the testing direction. This is probably because the excess binder at higher binder saturation spreads outside the edges of the printed sample, resulting in reduction of the linear dimensional accuracy.
2. The linear dimensional accuracy of the green samples exhibited an anisotropic behavior depending on the testing direction. The Z-direction always had the lowest linear dimensional accuracy, which may be associated with the different rates of binder penetrating in vertical (Z) direction and spreading in lateral (X and Y) directions. On the other hand, the X-direction always had the highest linear

dimensional accuracy, which may be because the X-direction (i.e., the binder jetting direction) is not affected by the powder spreading that takes place in Y-direction. This orthotropic behavior was true regardless of the binder saturation level, but more pronounced in the samples printed with Shell/Core of 1:2 than 1:1.

3. The compressive strength of the green samples also exhibited an orthotropic behavior depending on the testing direction. Regardless of the saturation level and shell to core ratio, the compressive strength in X-direction was always higher than in Z-direction, which may be related to the preferential orientation of the powder particles during the powder spreading process. This orthotropic behavior was more pronounced in the samples printed with Shell/Core of 1:2 than 1:1.
4. The change in the Shell/Core ratio from 1:1 to 1:2 significantly increased the compressive strength of the green samples. This is true regardless of the testing direction and binder saturation level.
5. In both X and Z directions, the increase in the binder saturation level significantly increased the compressive strengths. However, the rate of increase in the compressive strength of the green samples with Shell/Core of 1:2 was higher than that with Shell/Core of 1:1.
6. The inferior compressive strength of the green samples printed with lower binder saturation levels and shell to core ratios is probably due to incomplete hydration process due to insufficient amount of binder, which in turn results in a weak bond between the powder particles.

Future work will be focused on adjusting powder formulation and selecting effective post-processing method to improve the final characteristics of printed structures using the developed Portland cement-based powder.

References

1. Wohlers, T.: Wohlers Report 2016. Wohlers Associates Inc., Fort Collins (2016)
2. Nematollahi, B., Xia, M., Sanjayan, J.: In current progress of 3D concrete printing technologies. In: Proceedings of the International Symposium on Automation and Robotics in Construction (ISARC), Taipei (2017)
3. Nematollahi, B., Vijay, P., Sanjayan, J., Xia, M., Nerella, V.N., Mechtcherine, V.: Fresh and hardened properties of extrusion-based 3D printed geopolymer for construction applications. Materials (under review)
4. Nematollahi, B., Xia, M., Sanjayan, J.: Effect of type of fiber on inter-layer bond and flexural strengths of extrusion-based 3D printed geopolymer. In: Proceedings of the 2nd International Conference on Advanced Manufacturing and Materials (ICAMM), Tokyo (2018)
5. Cesaretti, G., Dini, E., De Kestelier, X., Colla, V., Pambaguian, L.: Building components for an outpost on the Lunar Soil by means of a novel 3D printing technology. *Acta Astronaut.* **93**, 430–450 (2014)
6. Rael, R., San Fratello, V.: Developing concrete polymer building components for 3D printing. In: Proceedings of the 31st Annual Conference of the Association for Computer Aided Design in Architecture (ACADIA), Banff (2011)
7. Nematollahi, B., Sanjayan, J., Shaikh, F.U.A.: Synthesis of heat and ambient cured one-part geopolymer mixes with different grades of sodium silicate. *Ceram. Int.* **41**, 5696–5704 (2015)

8. Xia, M., Sanjayana, J.: Method of formulating geopolymer for 3D printing for construction applications. *Mater. Des.* **110**, 382–390 (2016)
9. Xia, M., Sanjayana, J.: Post-processing methods for improving strength of geopolymer produced using 3D printing technique. In: International Conference on Advances in Construction Materials and Systems, ICACMS, Chennai (2017)
10. Xia, M., Nematollahi, B., Sanjayana, J.: Printability, accuracy and strength of fly ash/slag geopolymer made using powder-based 3D printing for construction applications. *Autom. Constr.* (under review)
11. Xia, M., Nematollahi, B., Sanjayana, J.: Influence of binder saturation level on compressive strength and dimensional accuracy of powder-based 3D printed geopolymer. In: Proceedings of the 2nd International Conference on Advanced Manufacturing and Materials (ICAMM), Tokyo (2018)
12. Biernacki, J.J., Bullard, J.W., Sant, G., Brown, K., Glasser, F.P., Jones, S., Ley, T., Livingston, R., Nicoleau, L., Olek, J., Sanchez, F., Shahsavari, R., Stutzman, P.E., Sobolev, K., Prater, T.: Cements in the 21st century: challenges, perspectives, and opportunities. *J. Am. Ceram. Soc.* **100**(7), 2746–2773 (2017)
13. Gibbons, G.J., Williams, R., Purnell, P., Farahi, E.: 3D printing of cement composites. *Adv. Appl. Ceram.* **109**(5), 287–290 (2010)
14. Maier, A.-K., Dezmirean, L., Will, J., Greil, P.: Three-dimensional printing of flash-setting calcium aluminate cement. *J. Mater. Sci.* **46**(9), 2947–2954 (2010)
15. Suwanprateeb, J., Sangam, R., Panyathanmaporn, T.: Influence of raw powder preparation routes on properties of hydroxyapatite fabricated by 3D printing technique. *Mater. Sci. Eng. C Mater. Biol. Appl.* **30**(4), 610–617 (2010)
16. Castilho, M., Gouveia, B., Pires, I., Rodrigues, J., Pereira, M.: The role of shell/core saturation level on the accuracy and mechanical characteristics of porous calcium phosphate models produced by 3D printing. *Rapid Prototyp. J.* **21**(1), 43–55 (2015)
17. Fielding, G.A., Bandyopadhyay, A., Bose, S.: Effects of silica and zinc oxide doping on mechanical and biological properties of 3D printed tricalcium phosphate tissue engineering scaffolds. *Dent. Mater.* **28**(2), 113–122 (2012)
18. Shanjani, Y., Hu, Y., Pilliar, R.M., Toyserkani, E.: Mechanical characteristics of solid-freeform-fabricated porous calcium polyphosphate structures with oriented stacked layers. *Acta Biomater.* **7**(4), 1788–1796 (2011)
19. Stopp, S., Wolff, T., Irlinger, F., Lueth, T.: A new method for printer calibration and contour accuracy manufacturing with 3D-print technology. *Rapid Prototyp. J.* **14**(3), 167–172 (2008)